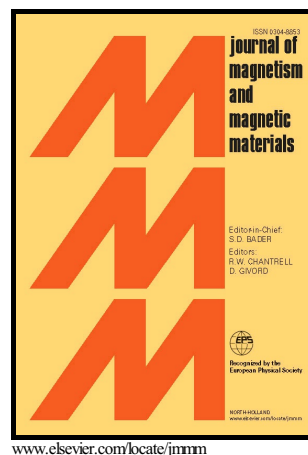# Author's Accepted Manuscript

Facile microwave synthesis of uniform magnetic nanoparticles with minimal sample processing

Thomas Schneider, Anna Löwa, Stoyan Karagiozov, Lisa Sprenger, Lucía Gutiérrez, Tullio Esposito, Gernot Marten, Katayoun Saatchi, Urs O. Häfeli

Cite this article as: Thomas Schneider, Anna Löwa, Stoyan Karagiozov, Lisa Sprenger, Lucía Gutiérrez, Tullio Esposito, Gernot Marten, Katayoun Saatchi and Urs O. Häfeli, Facile microwave synthesis of uniform magnetic nanoparticles with minimal sample processing, *Journal of Magnetism and Magnetic Materials*, http://dx.doi.org/10.1016/j.jmmm.2016.07.063

# *Facile Microwave Synthesis of Uniform Magnetic Nanoparticles with Minimal Sample Processing*

Thomas Schneider,[a,*] Anna Löwa,[a] Stoyan Karagiozov,[a] Lisa Sprenger,[a,b] Lucía Gutiérrez,[c] Tullio Esposito,[a] Gernot Marten,[a] Katayoun Saatchi,[a] Urs O. Häfeli [a,*]

[a] Faculty of Pharmaceutical Sciences, University of British Columbia, Vancouver, BC V6T 1Z3, Canada

[b] TU Dresden, Chair of Magnetofluiddynamics, Measuring and Automation Technology, 01062 Dresden, Germany

[c] Instituto Universitario de Nanociencia de Aragón (INA), University of Zaragoza, 50018 Zaragoza, Spain

Contact Information:

*Corresponding Authors: Thomas Schneider † (tom.schneider@ubc.ca), Urs Hafeli (urs.hafeli@ubc.ca)

Present Address: †Department of Chemistry, University of Washington, Seattle, USA.

**Abstract**

We present a simple and rapid method for the synthesis of small magnetic nanoparticles (diameters in the order of 5-20 nm) and narrow size distributions (CV's of 20-40%). The magnetite nanoparticles were synthesized in green solvents within minutes and the saturation magnetization of the particles was tunable by changes in the reaction conditions. We show that this particle synthesis method requires minimal processing steps and we present the successful coating of the particles with reactive bisphosphonates after synthesis without washing or centrifugation. We found minimal batch-to-batch variability and show the scalability of the particle synthesis method. We present a full characterization of the particle properties and believe that this synthesis method holds great promise for facile and rapid generation of magnetic nanoparticles with defined surface coatings for magnetic targeting applications.

**Keywords**

**Introduction**

Drug delivery is an important method in the fight against cancer and other diseases as it increases specificity between the target site and the drug, thereby lowering side effects due to whole body drug exposure. Different vectors that interact with a target site in the body (*e.g.*, an inflamed

tissue) can facilitate drug delivery. Magnetic nanoparticles (MNPs) can be used as such vectors and can be guided and enriched at the target site by directed magnetic fields [1]. Magnetic drug targeting is a recent drug delivery method where the drug is bound to the MNPs and, after delivery to the target, is released to induce a therapeutic effect [2]. Different factors can impact the quality of the magnetic drug carrier, which include its size distribution and composition, its cell permeability and especially its protective coating and release characteristics of the bound drug. A major challenge in the development of magnetic drug carriers for clinical therapy has been the poor particle size distribution of MNPs, methods producing large amounts of particles per batch, and the poor mass throughput of methods producing MNPs with excellent size distributions [3]. In addition, the protective coating of the MNPs needs to be multifunctional; that is it needs to be a thin biocompatible coating and it needs to facilitate peptide and antibody conjugation, as well as encapsulate/bind and controllably release a drug.

Conventional methods to synthesize MNPs that have high yields include microemulsion syntheses [4] and wet chemical methods based on iron salt solutions through co-precipitation or thermal decomposition from organometallic solvent solutions [5,6]. The latter method has gained attraction as a fast synthetic strategy to create uniform MNPs, but requires high temperatures, toxic chemicals, and the addition of stabilizing agents [7–10]. Over the past years, solvothermal synthetic strategies have been studied in detail [11], particularly with a focus on low cost precursor materials including iron pentacarbonyl [7], iron oleate [12], iron(II) acetate [9], and iron(III) acetylacetonate [8]. The main advantage of solvothermal synthesis is the high level of control over the reaction conditions. But the use of toxic and combustible solvents (*e.g.*, benzyl ethers or octadecene) limits the application of particles created by this method. The use of these particles in biological applications such as magnetic drug targeting requires extensive post-

processing to separate the MNPs from toxic solvents and residual stabilizing agents, and it often requires further wet chemical methods to create biocompatible and functional coatings. All these steps increase the time required to create functionalized and biocompatible MNPs. In addition, the use of different solvents for MNP synthesis and subsequent coating can create challenges in terms of solubility mismatches between MNPs and coating materials, changes in colloidal stability of the particles, and low yield of the final coated biocompatible MNPs. To overcome these limitations and increase the versatility and applicability of MNPs as magnetic drug carriers in *in vivo* applications, it is desirable to take advantage of the wealth of available methods for particle synthesis and to minimize the overall processing steps (*i.e.*, reduction in centrifugation and washing steps), thereby creating a one-pot synthetic method with high control over the particle quality, high yield, and high mass throughput per particle batch.

Recent advances in novel microwave-based synthetic methods [13–15] provide the foundation to design simplified synthetic strategies that take advantage of isochoric reaction conditions and so called greener solvents. Greener solvents are less toxic, produce fewer harmful byproducts, and are favorable in synthetic chemical methods aimed at biological applications. Among the greener solvents are dihydroxy alcohols, including triethylene glycol (TEG), whose physicochemical properties are favorable for solvothermal decomposition methods (*i.e.*, high viscosities and boiling points). TEG is typically used as a plasticizer [16] as well as a dehydration solvent in the gas industry [17]. It is also known to be a mild disinfectant and shows no known toxicities unlike the related di(ethylene glycol) [18,19]. In addition, its high solubility in water is ideal to simplify sample post-processing steps. Other alcohols suitable for solvothermal decomposition due to their high viscosities and boiling points include benzyl alcohol, which is immiscible in water. Synthesis of MNPs with benzyl alcohol and triethylene glycol as solvents has been shown to

yield uniform MNPs in autoclaves [20–23] and by microwave-based methods [24,25]. However, all these methods required several processing steps followed by multiple washing and (often) centrifugation steps to separate the MNPs from the solvents. Microwave based MNP synthesis was also shown from aqueous $Fe^{2+}$ and $Fe^{3+}$, resulting in $\gamma$-$Fe_2O_3$ and $\alpha$-$Fe_2O_3$ MNPs [26,27], which exhibit lower saturation magnetization than $Fe_3O_4$.

Here we present a fast method to produce large quantities of functionalized MNPs for the use as magnetic drug carrier precursors with excellent size distributions by a combination of facile microwave synthesis and a bisphosphonate coating strategy. The bisphosphonate coating provides an active amine group for conventional amine-reactive crosslinker chemistry [28], which is ideal for functional bioconjugation to cell permeable proteins, antibodies, and drugs. The particles created by this one-pot synthetic method are uniform in size and shape, water soluble, and contain mainly magnetite, as supported by full particle characterization.

**Materials and Methods**

Particle Synthesis & Coating

Microwave synthesis experiments were conducted in an Initiator$^+$ (Biotage Sweden AB, Uppsala, Sweden). All experiments were conducted with a solution of iron acetylacetonate (Fe(acac)$_3$; Fe(C$_5$H$_7$O$_2$)$_3$; cat. F300; Sigma Aldrich Ltd., Oakville, ON, Canada) in tri(ethylene glycol) (cat. #T59455, Sigma Aldrich) under inert conditions. Prior to the synthesis, the Fe(acac)$_3$ was mixed in Biotage microwave vials together with the solvent and sealed with vial caps. Typical reaction volumes were 2 mL, but larger reaction volumes (up to 20 mL) were used in scale-up studies.

A customized $N_2$ – flood system was used to blanket the solution with $N_2$ for 30 min (**Fig. 1**). The Fe(acac)$_3$ was then converted into magnetic nanoparticles through thermal decomposition in the Initiator$^+$ by first heating to 200°C for up to 24 h ($t_h$) followed by reflux heating to 250°C for up to 24 h ($t_{rf}$). The total reaction time is given as the sum of $t_h$, $t_{rf}$, and the time used for heating and cooling to the pre-set temperatures (typically 5-10 min).
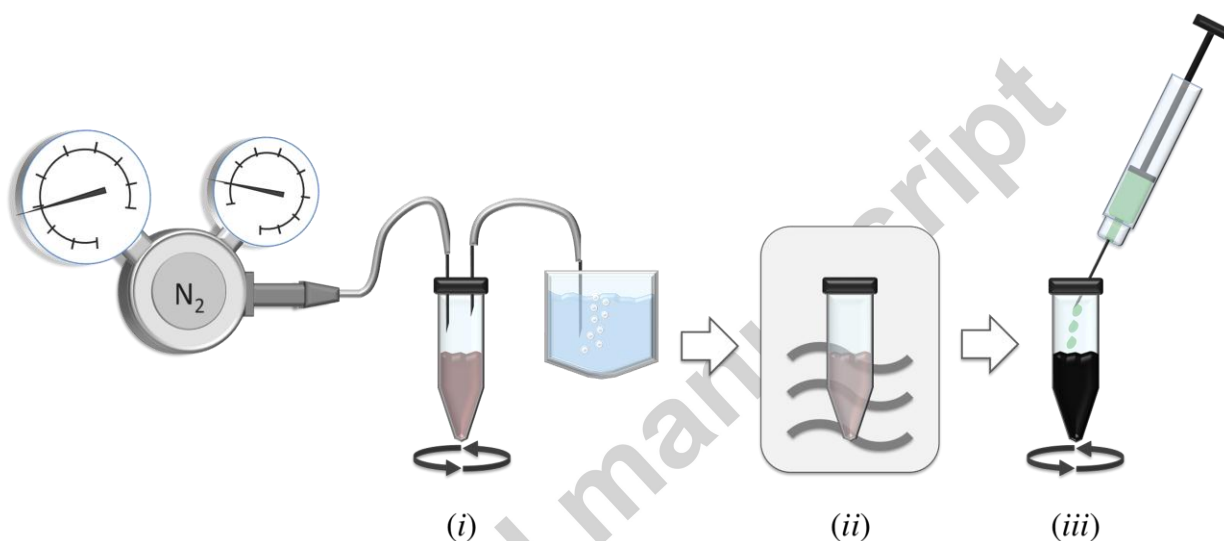
(i)   (ii)   (iii)

Figure 1. General process flow in the particle synthesis: (i) The precursor iron salt is dissolved under inert conditions, (ii) undergoes thermal decomposition in a microwave oven resulting in the formation of nanoparticles, (iii) which are coated directly in the reaction vessel (one pot method). Subsequent precipitation and separation/washing using a magnet or centrifuge yields stable water-soluble particles.

The particles were coated directly in the microwave vials by injecting alendronic acid (cat. #A2120, 98% pure; TCI America, Portland, OR, USA) through the vial cap's occulum. The alendronic acid solution was prepared fresh the same day of coating in ultrapurified water

(MilliQ, Millipore Corp., Milford, MA) at a concentration of 5 mg/mL aided by sonication for 60 min. The particles were then separated and prepared for analysis by precipitation in ethyl acetonate, followed by centrifugation at 8,200×$g$ for 10 min. This process was repeated and the particles redispersed in water or dried under nitrogen for analysis.

Particle Bioconjugation

Different stock solutions were prepared on the day of the conjugation. A stock solution of 0.5 M MES buffer (2-(N-morpholino) ethanesulfonic acid (MES); cat. # M3671; Sigma Aldrich Ltd.) at pH 3-4 was prepared in distilled water. The conjugation buffer consisted of 6 mg/mL EDC (N-(3-dimethylamino-propyl)-N′-ethylcarbodiimide hydrochloride; cat. # E7750; Sigma Aldrich Ltd.) and 12 mg/mL NHS (N-hydroxy-succinimide; cat. # 130672; Sigma Aldrich Ltd.) dissolved in MES buffer. A stock solution of 4 mg/mL rhodamine B (cat. # R6626, Sigma Aldrich Ltd.) was prepared in MES buffer.

Alendronate coated magnetic nanoparticles (alendronate-MNPs) were washed twice in ethyl acetate and subsequently dried. The particles were then resuspended in ultra purified water (18.2 MΩ; MilliQ; Millipore Corp.) to achieve a concentration of 20 mg/mL and dispersed by sonication for 25 min. An aliquot of 1 mg particle dry weight was then mixed with 0.5 mL conjugation buffer (10 mg/mL EDC, 20 mg/mL NHS in MES) and 2 mg of rhodamine. The mixture was incubated for 30 min on a rotor after which the sample was titrated to pH 7.6 with 5 M NaOH. After 1 hour incubation the sample was removed from the rotor and dialyzed for 5 days (Spectra/Por Dialysis Membrane, MWCO 1,000 Da; cat. #132638; Spectrum Labs, Irving, TX). Subsequently, the sample was recovered and resuspended in 0.5 mL ultra purified water

followed by sonication for 5 min. The rhodamine-coated MNPs were washed once in water by centrifugation (14,000 rpm, 15 min; Model 5415, Eppendorf AG; Hamburg, Germany), dried, and stored until further analysis.

In vitro viability testing by MTT assay

Pristine magnetic nanoparticles synthesized for 30 min and 48 h were precipitated by acetone, washed twice, and dried. The dried particles were re-dispersed into ultrapurified water at a concentration of 1 mg/mL and sonicated for 30 min on ice. The re-dispersed samples were analyzed by DLS for particle size and Zeta potential (Nano ZS; Malvern Instruments Ltd, Worcestershire, UK). Before in vitro testing, the particle samples were sterile filtered (0.22 μm Millex®GP filter units; Millipore, Billerica, MA, USA). The particles were then diluted with culture media before assessment by MTT assay.

Cell viability MTT assays were conducted to investigate the effect of the particles at different concentrations on the viability of cancer cells. Human prostate cancer cells (PC-3; ATCC CRL-1435TM; American Type Culture Collection, Manassas, VA, USA) and mouse embryo fibroblast cells (NIH/3T3; ATCC® Number: CRL-1658TM; ATCC) were cultured in 75 cm$^2$ tissue culture flask (Falcon$^{TM}$; cat.# 430641 Corning Inc., Corning, NY, USA) according to protocols provided by the ATCC. The PC-3 cells were subcultured in F-12K Medium (cat. #21127022; Invitrogen Corporation; Carlsbad, CA), while the NIH/3T3 cells were subcultured in Dulbecco's Modified Eagle's Medium (DMEM; ATCC® Number: 30-2002; ATCC). All media were supplemented with 10% fetal bovine serum (FBS; cat. # 12483-020; Invitrogen Corp.) and 1% Penicillin/Streptomycin (Penicillin-Streptomycin 10,000 units/mL penicillin, 10 mg/mL

streptomycin; cat. #10378-016; Invitrogen Corp.). The cells were subcultured in an incubator at constant humidity, 5% $CO_2$, and 37°C.

For the MTT assay, the cells were harvested aided by trypsin and resuspended in the required volume of culture media. The cell concentration was subsequently evaluated using a hemacytometer (AO Spencer Bright-Line, St. Louis, MO). Aliquots of 100 µL cell stock solution were transferred into a 96-well plate (Microtest 96; cat. # 353072, BD Bioscience, Bedford, MA) giving a seed concentration of 1,250 cells/well. The cells were then cultured for 24 h at constant humidity, 5% $CO_2$, and 37°C. After the culture period, 100 µL aliquots of the particle suspensions in the respected media were added to the wells without removal of the media in the wells and the cells were subsequently incubated with the MNPs for 22 h. The MTT stock solution was prepared by dissolving 5 mg/mL thiazolyl blue tetrazolium bromide (cat.# M2128; Sigma Aldrich, Inc.) in phosphate buffered saline ($1\times$ PBS). The solution was sonicated for 15 min followed by sterile filtration through a syringe filter. On the final day of the assay, 20 µL of the MTT stock solution was added to each well and the 96-well plate was shaken for 30 s on the plate reader. The 96-well plates were then incubated at 37°C in an incubator for 3 h. Finally, the solution was removed completely from each well and replaced by 150 µL of DMSO, shaken for 30 s on the plate reader, followed by incubation for 1 h in the dark at room temperature. The resulting color change was evaluated at 540 nm using multiscanner (Multiscan Ascent; Labsystems, Helsinki, Finland).

Transmission Electron Microscopy

Transmission Electron Microscopy was conducted on a Hitachi 7600 with an AMT Advantage (1 megapixel) CCD camera (Hamamatsu ORCA). Small aliquots of the samples were first washed twice by precipitation with ethyl acetate and centrifugation at $8,200 \times g$ for 10 min. The samples were resuspended in chloroform and pipetted onto TEM grids (PELCO® Formvar/Carbon 200 mesh TH; cat. #01803-F, Ted Pella, Inc., Redding, CA, USA). The particle size and size distribution of $n > 2,300$ particles was then assessed and measured aided by a customized particle imaging algorithm (LabVIEW, National Instruments Corporation, Austin, TX, USA).

Dynamic Light Scattering and Zeta Potential

The particle size distribution and Zeta potential was measured on a Zetasizer Nano ZS (Malvern Instruments Ltd, Worcestershire, UK) using acrylic cuvettes (4 mL, square cuvette; cat. #67.755; Sarstedt INC, Newton, NC, USA) and folded capillary cells (cat. # DTS1070; Malvern Instruments Ltd), respectively. The parameters used for the dynamic light scattering (DLS) measurements were $n_{TEG} = 1.4559$, $\eta_{TEG} = 49.00$ cP, $n_{FeOx} = 2.4200$, abs. $= 0.200$.

The isoelectric points of MNP samples were determined by titration and measuring the respective Zeta potentials of the samples. The washed MNP samples were first resuspended in ultrapurified water, followed by bath-sonication for 10 min. The samples were titrated using 0.1 M NaOH and 0.1 M HCl over a range between pH $= 2$ and 12 (SG2-ELK $-$ SevenGo™ pH meter with an InLab® Micro Electrode; Mettler-Toledo Inc., Columbus, OH, USA). All measurements were conducted in triplicate (minimum of 10 measurements each).

Fourier Transform – Infrared Spectroscopy

Fourier Transform – Infrared (FT-IR) spectroscopy was conducted on a Spotlight 400 FTIR Imaging System (Perkin Elmer, Waltham, MA, USA). Dry particle samples were measured on an Attenuated Total Reflectance (ATR) crystal and the spectra were acquired at a wavenumber range from $650 - 4,000$ cm$^{-1}$ and with four (4) cumulative scans at a resolution of 4 cm$^{-1}$. Finally, the spectra were ATR corrected using an algorithm provided by Perkin Elmer.

Magnetic Property Characterization

Magnetic properties of the samples were measured using a Vibrating Sample Magnetometer (VSM; LakeShore 7400 Series, Lake Shore Cryotronics, Inc., Westerville, OH, USA) at room temperature. The viscosity of the samples was measured by rheometry (Physica MCR301 rheometer; Anton Paar USA Inc., Ashland, VA, USA) and used to determine sample density, shear flow, saturation magnetization, and particle size distribution based on a method by Weser and Stierstadt [29].

The samples were also characterized using a Superconducting Quantum Interference Device (SQUID) Magnetometer. The samples were prepared by impregnating a piece of cotton with a small aliquot of particle suspension. The impregnated piece of cotton was then placed in a gelatin capsule for magnetic characterization. The field dependent magnetization measurements were performed in a MPMS-5S SQUID Magnetometer (Quantum Design Inc., San Diego, CA, USA) at 300 K up to 5 T. MNP powders were weighed and digested with nitric acid (1 h at 90 ºC) and Inductively Coupled Plasma – Optical Emission Spectrometry (ICP-OES) was used to measure

the iron content in the samples calibrated against standard solutions in an OPTIME 2100DV (Perkin Elmer).

X-Ray Diffraction Analysis

X-Ray Diffraction (XRD) analysis of dried samples was conducted with Cu radiation on a Bruker D8-Advance (Bruker Canada, Milton, ON, CAN) equipped with a LynxEye silicon strip, a Ni filter (to strip out the CuKbeta radiation), and Bragg-Brentano configuration.

Differential Scanning Calorimetry

Thermal properties of the MNPs and MNPs coated with alendronate were investigated by Differential Scanning Calorimetry (DSC) analysis on a DSC Q100 (TA Instruments, New Castle, DE, USA). The samples were placed in hermetic aluminum pans and heated to 500°C at a rate of 20°C/min at constant nitrogen flow of 50 mL/min. After a one minute isothermal step, the samples were cooled at a rate of 20°C/min.

**Results and Discussion**

Synthesis and Particle Size Distribution

The MNPs synthesized by the microwave-based method presented here in TEG showed small sizes and relatively narrow size distributions. We tested different reaction conditions and the heating duration was varied to investigate changes in the particles' properties. Both, TEM

imaging and Dynamic Light Scattering analysis were used to characterize the particle sizes and shapes.

The particles synthesized by our method are round with irregular shapes as shown by TEM imaging (**Fig. 2**). With increasing duration for the heating and reflux heating, the particle size increased from $6.2 \pm 1.5$ nm ($t = 30$ min; **Fig. 2a**) to $12.3 \pm 3.4$ nm ($t = 48.3$ h; **Fig. 2e**) based on size analysis of TEM images. The measurements by dynamic light scattering show a larger size of the particles (*e.g.*, $9.6 \pm 3.6$ nm for $t = 30$ min; **Fig. 2f**) compared to TEM measurements. This was expected as the scattering analysis by the DLS includes the measurement of solvent layers adsorbed to the particles, while sizes measured from TEM are only from the iron oxide core. It can be seen that with increasing heating durations ($t_h$, $t_{rf}$) the particle size increases in the measurements by DLS and by TEM, but the increase was found to be stronger in the particles measured by DLS with average sizes of up to $24.4 \pm 9.1$ nm for $t = 48.3$ h (**Fig. 2f**). It has to be noted that the particle samples for the longest heating duration ($t = 48.3$ h) showed large clusters in the TEM samples (see **Fig. 2e**) and the image analysis from TEM images with the custom particle imaging algorithm was not feasible for this parameter. Instead the particles were measured manually for this parameter (n = 250).
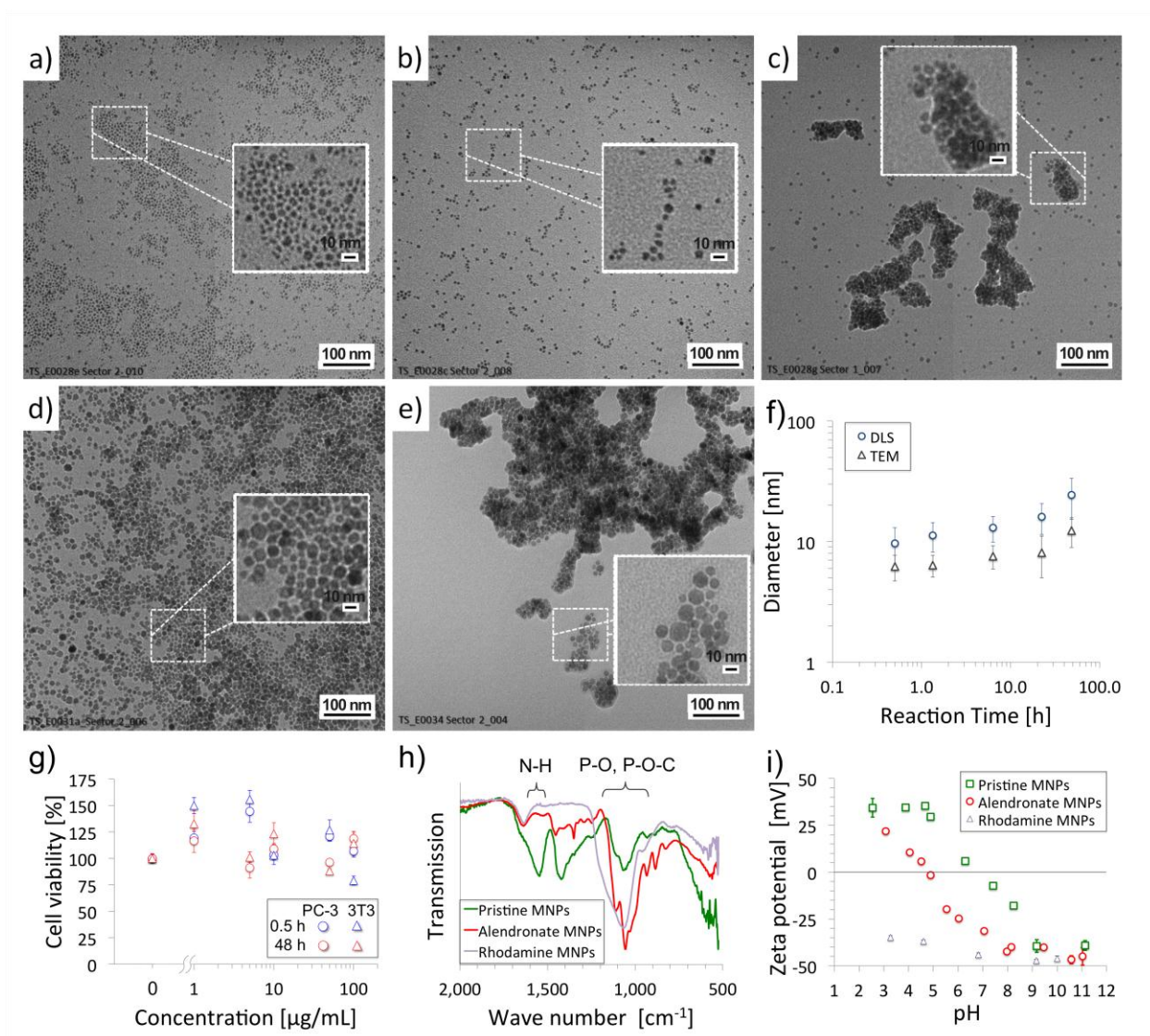
Figure 2. TEM Images of MNPs synthesized with reaction times of (a) 0.5 h, (b) 1.3 h, (c) 6.3 h, (d) 22.3, and (e) 48.3 h. The particle size distributions measured by DLS and TEM (n > 2,300) are shown in (f). The scale bars in images (a-e) correspond to 100 nm, while the ones in the insets correspond to 10 nm. Biocompatibility test of MNPs in vitro with particles synthesized for 30 min and 48.3 h are shown for PC-3 cells and NIH/3T3 cells (g). Note that the particle concentration is shown on a logarithmic scale after the broken axis. FTIR analysis (h) and

titrated Zeta potential (i) of pristine MNPs (green), alendronate coated MNPs (red), and rhodamine labeled MNPs (purple).

Overall, it was found that the particle size distribution increased slightly with increasing reaction time, both in measurements by TEM and DLS. The increase in the particle's CV's measured for reaction times of $t = 30$ min to $t = 48.3$ h was from 24.1% to 39.1% for TEM analysis and from 35.4% to 37.4% for DLS analysis. The overall batch-to-batch variability was found to be small for the same reaction parameters (*i.e.*, heating duration, precursor concentration, reaction volume). To further test the scalability of the method we varied the precursor concentration and reaction volume, which provides a scaling factor of 500 in terms of mass throughput. We found that with increasing precursor concentration from 0.01 M to 0.50 M the particle size became more disperse, while the samples showed similar average particle diameters between 7.1 nm to 8.9 nm (**Fig. 3a**).

Moreover, a 10-fold increase in reaction volume showed an increase in particle size distribution (**Fig. 3b,c**). This increase in particle CV was related to fluctuations in the reaction conditions, which was caused by fluctuations in the heating of the larger 20 mL vials in the Initiator[+] when compared to 2 mL vials used in most of the studies presented here (graphs in **Fig. 3b,c**).

The challenges in heating larger vials are thought to be due to stronger thermal gradients that develop within the vials. The temperature of the reaction solution is measured by IR directly at the outer glass surface of the vials. We encountered a delay in the respective feed-back control to the microwave radiation required to maintain a set temperature in our studies with iron salt solutions. Strong fluctuations, however, were only found in experiments with large vials. In

smaller vials (2 mL), the temperature was maintained by the Initiator[+] at or near the pre-set temperature for over 48 h. For example, we found that for a pre-set temperature of 250°C the temperature varied only by ±2.4°C over 24 h. Aside from the increase in particle dispersity, the microwave synthesis method presented here provides the ability for a significant scale-up in mass throughput. By both increasing the reaction volume and the precursor concentration, the particle throughput can be scaled from a few milligrams to 10's of grams of MNPs per batch.
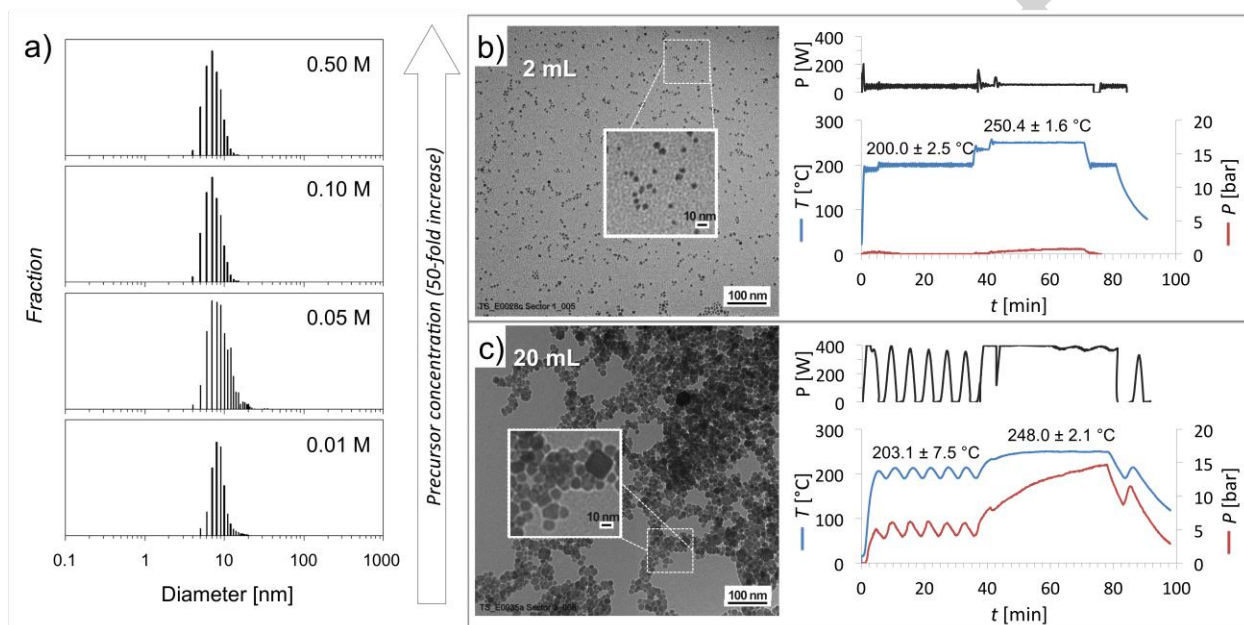


Figure 3. Scale up in reaction conditions and the effect on particle size (by TEM): Change in precursor concentration (a) and changes on reaction volume (b,c). Graphs in (b,c) show the trace of power input, temperature, and pressure in the reaction vial during a typical synthesis. The study with changes in precursor concentration were conducted with a sample volume of 2 mL and at a total reaction time of 1.3 h.

Biocompatibility

The effect of the particles' dispersity and cytotoxicity was investigated by *in vitro* MTT assays with a focus on the toxicity of MNPs synthesized for 30 min and 48.3 h. We found in our study no effect on cell viability when pristine MNPs synthesized for 30 min and 48 h were applied *in vitro* to NIH/3T3 and PC-3 cell lines up to a concentration of 100 μg Fe / mL (**Fig. 2g**). The toxicological effects of TEG coated MNPs in our study were comparable to similar studies using MTT assays in HeLa, U87MG, and HepG2 cell lines [30]. Our MNPs are thus biocompatible at concentrations up to at least 100 μg Fe / mL.

FT-IR Analysis & Zeta Potential

The particles were coated directly in the vial after completion of the synthesis by injecting alendronic acid. This one-pot synthesis and coating has the advantage of eliminating time intensive washing and purification steps used in conventional methods. FT-IR spectral analysis was used to characterize the success of the coating (**Fig. 2h**). Furthermore, the successful coating was also verified by taking advantage of changes in the particle's Zeta potential due to the presence of alendronate on the particle surface (**Fig. 2i**).

The FT-IR spectra of pristine MNPs (green line in **Fig. 2h**) show strong peaks between 1,150 – 1,040 cm$^{-1}$, which can be attributed to triethylene glycol (TEG), the solvent used for synthesis. In addition, structural peaks between 1,500 – 1,250 cm$^{-1}$, and between 3,500 – 2,800 cm$^{-1}$ (data not shown) indicate the presence of TEG on the particle surface after synthesis. Similar peaks that can be associated with the presence of TEG are found in the spectra of alendronate coated MNPs, indicating residual TEG on the particles after washing in ethyl acetate (red line in **Fig. 2h**). This is in good agreement with the increases in particle size with increasing reaction

duration as measured by DLS (blue circles in **Fig. 2f**). It is hypothesized that TEG forms EG layers on the particles, which after washing allow dispersion of the particles in water. The cropped peak below 800 cm$^{-1}$ can be attributed to Fe. However, a detailed FT-IR analysis below 600 cm$^{-1}$ was not possible in our study. The successful coating of the MNPs by alendronate is reflected in the change of the wide P-O and P-O-C stretching vibrational peaks between 1,150 – 965 cm$^{-1}$, and indicate good binding of the phosphonate to the surface of the MNPs (red line in **Fig. 2h**). In addition, the presence of a peak representing the amine group (1,650 – 1,560 cm$^{-1}$) is found in both, free alendronate (not shown) and alendronate coated MNPs, but not pristine (uncoated) MNPs. This is further support that the coating was successful and that the functional amine group remains intact.

In addition to FTIR characterization of the particle's surface, the change in the isoelectric point of the particle sample can be used to determine the success of surface modifications. The pH dependent Zeta potential of pristine (uncoated) and alendronate functionalized particles was measured in a titration study with HCl and NaOH. At neutral pH of 7.4 pristine MNPs were slightly negatively charged at -7.24 mV, while alendronate particles had a surface charge of -35.9 mV (based on linear interpolation; green squares versus red circles in **Fig. 2i**). The lower surface charge in alendronate particles was expected resulting from the highly charged alendronate that binds through its bisphosphonate to the MNP's iron surface leaving a deprotonated hydroxyl group exposed. A shift of the isoelectric point from pH 6.8 (pristine MNPs) to pH 4.8 (alendronate coated MNPs) is further evidence of the successful surface modification of the MNPs with alendronate. This result is in good agreement with similar measurements of alendronate modified MNPs [31].

To proof that the primary amines on the alendronate coating of the MNPs are available for bio-functionalization, we conjugated rhodamine B to the alendronate MNPs through amide bonds. The resulting particles showed a further reduction of the particles' charge, as expected (purple triangles in **Fig. 2i**). The particles were readily dispersed in water aided by sonication and remained stable in solution for a few days. The particles formed clusters of particles with average size measured by DLS of $249.5 \pm 84.6$ nm, indicating aggregation of the particles after functionalization.

Magnetic Property Characterization

The magnetic properties of particles synthesized at different reaction conditions were characterized by vibrating sample magnetometry and state of the art Superconducting Quantum Interference Device (SQUID) Magnetometry. SQUID was used to investigate the changes in the magnetic properties with varying reaction conditions. No sizeable hysteresis was observed for any of the samples corroborating their superparamagnetic behavior at room temperature. The saturation magnetization ($M_{sat}$) of the particles correlated with heating duration. With increasing heating duration, $M_{sat}$ increased from 39.6 to 64.9 $Am^2/kg$ $Fe_3O_4$ after 30 min and 48.3 h, respectively (**Fig. 4**).

This fact is explained by the reduction of spin canting effects at the surface due to the decrease of the surface area/volume ratio. In addition, an increase of the initial susceptibility with increasing reflux time, as the particle size increases, was observed. Similar observations were previously described for particles with varying core sizes [32].
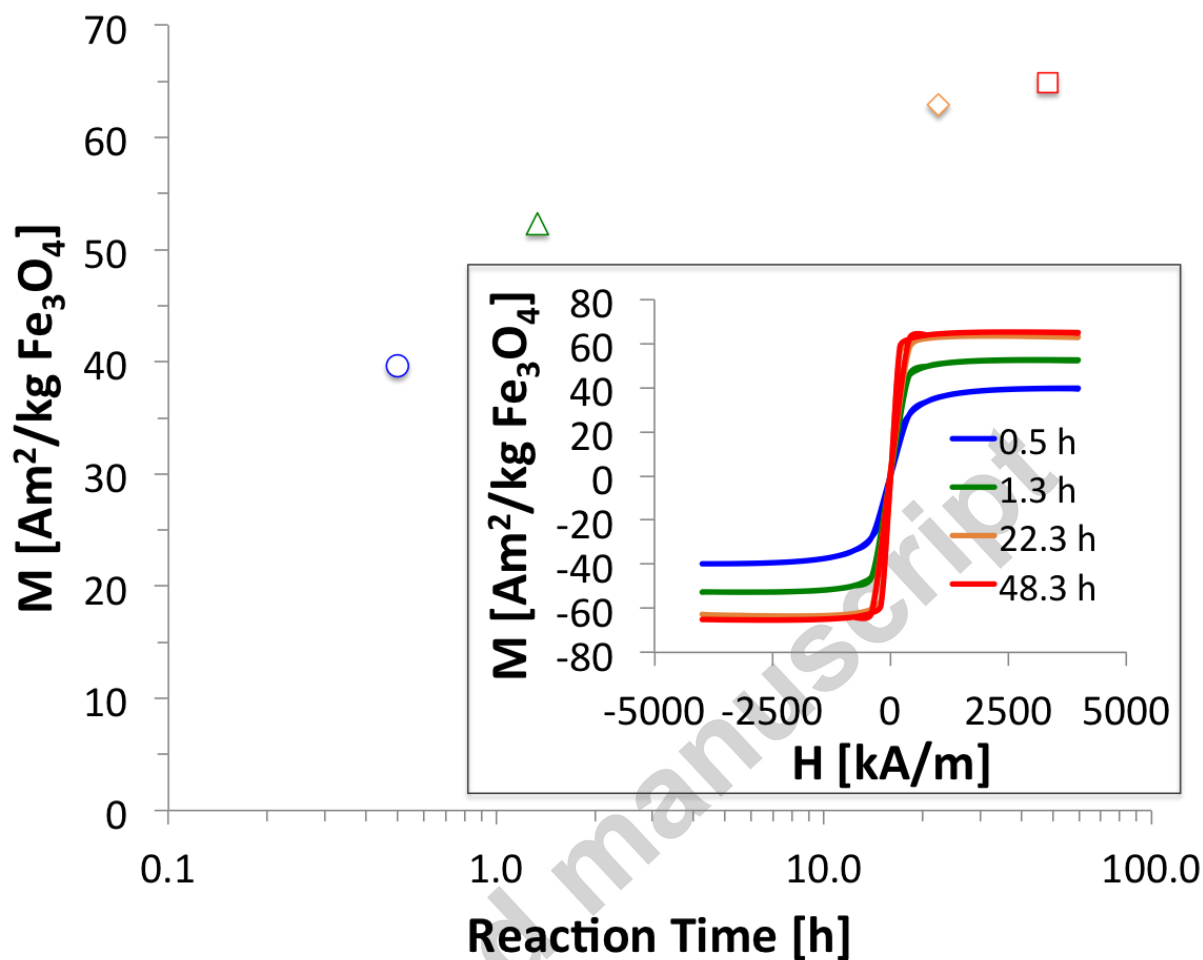
Figure 4.    Effect of reaction time for MNP synthesis on resulting sample magnetization (M). Inset shows the reaction time dependent H-M hysteresis measured by VSM for changing magnetic field (H).

VSM measurements were used to characterize the particle size distribution from scale-up experiments based on the Langevin function. We found that the particle size distribution as measured by TEM and DSL agreed well with the size distribution calculated from the VSM measurements (see **Fig. S1**). We quantified the size and size distribution both from dried

particles (by TEM) and in solution by dynamic light scattering and vibrating sample magnetometry. Based on the VSM measurements it was found that the particles were primarily composed of magnetite. The VSM measurements were conducted with samples obtained from scale-up experiments (t = 1.3 h) in a 10-fold larger reaction volume and resulted in a 18.5% higher $M_{sat}$ when compared to MNPs synthesized with the same reaction conditions, but with 2 mL reaction volumes as measured by SQUID. It has to be noted, however, that these measurements were conducted by different magnetic characterization methods (VSM versus SQUID) and different volumes were required for each method (mL versus µL). In addition, the reaction volumes for the synthesis were different. Overall, the $M_{sat}$ values measured for the two reaction volumes 2 mL versus 20 mL were similar and the differences in the measurements can be associated with differences in methodology and associated assumptions for the $M_{sat}$ calculations.

X-Ray Diffraction Analysis

The XRD study was conducted to further support the findings from the magnetic characterization (by VSM and SQUID measurements) and is strong support that the MNPs contained mainly magnetite. The standard XRD pattern for magnetite and maghemite are shown in **Fig. 5a** (black and brown bars, respectively). It can be seen that a distinction between the two phases, magnetite and maghemite, is rather difficult. The XRD pattern for maghemite exhibits additional peaks that are not present in the XRD pattern for magnetite, albeit these peaks are small and fall below the detection limit of many XRD instruments. The XRD spectra from samples representing five different reaction conditions are shown color-coded together with a sample of alendronate coated

MNPs (black line) in **Fig. 5a**. Our XRD analysis showed only peaks that could be attributed to magnetite or maghemite, while no peaks from other phases such as hematite or wüstite were detected. The characteristic peaks at (210) at 23.77° and (211) at 26.10° indicative of maghemite, were either not present or indistinguishable from the measurement background/noise in our XRD data (**Fig. 5a**). A closer look at characteristic peaks (400) and (511) show broader peaks with peak maxima correlating to those of magnetite (**Fig. 5b,c**). The differences in peak shift are particularly clear at peak (511) where the peak for magnetite is at $2\theta = 57°$, whereas the peak for maghemite is at $2\theta = 57.3°$. In addition, there is a decrease in peak base width with increasing heating duration, suggesting an increase in single-phase composition (**Fig. 5a**), while the peak center indicates primarily magnetite in all samples (see **Fig. 5b** and **c**). Furthermore, the use of alendronate as coating material seems not to diminish or affect the phase composition purely based on a comparison of the XRD spectra from coated (black line in **Fig. 5a**) and uncoated MNPs (light green line in **Fig. 5a**) of the same reaction duration.

In order to overcome challenges in characterizing samples that may contain either form of iron oxide, Kim et al.[33] proposed a stepwise screening through two characteristic peaks (e.g., peaks (400) and (511)). In their work they were able to calculate the ratio of magnetite to maghemite based on establishing calibration curves from pure samples of the two phases. Subsequently, the group applied a peak deconvolution scheme to the raw data to distinguish the two peaks.

Based on the calibration data and the peak intensity the group proposed that this method could be used to determine accurately the phase ratio in a sample. Although no step-wise scan around the peaks (400) and (511) were conducted in our study as proposed by Kim et al.[33], our XRD data showed only small widening peaks at the shortest reaction duration (t = 30 min), potentially

indicating a mixed composition of magnetite and maghemite in that sample. However, such peak widening (blue line in **Fig. 5b,c**) can be an artifact of the measurement. Overall, the XRD data suggests that for all other reaction conditions tested the main composition of MNPs synthesized by our method is magnetite.
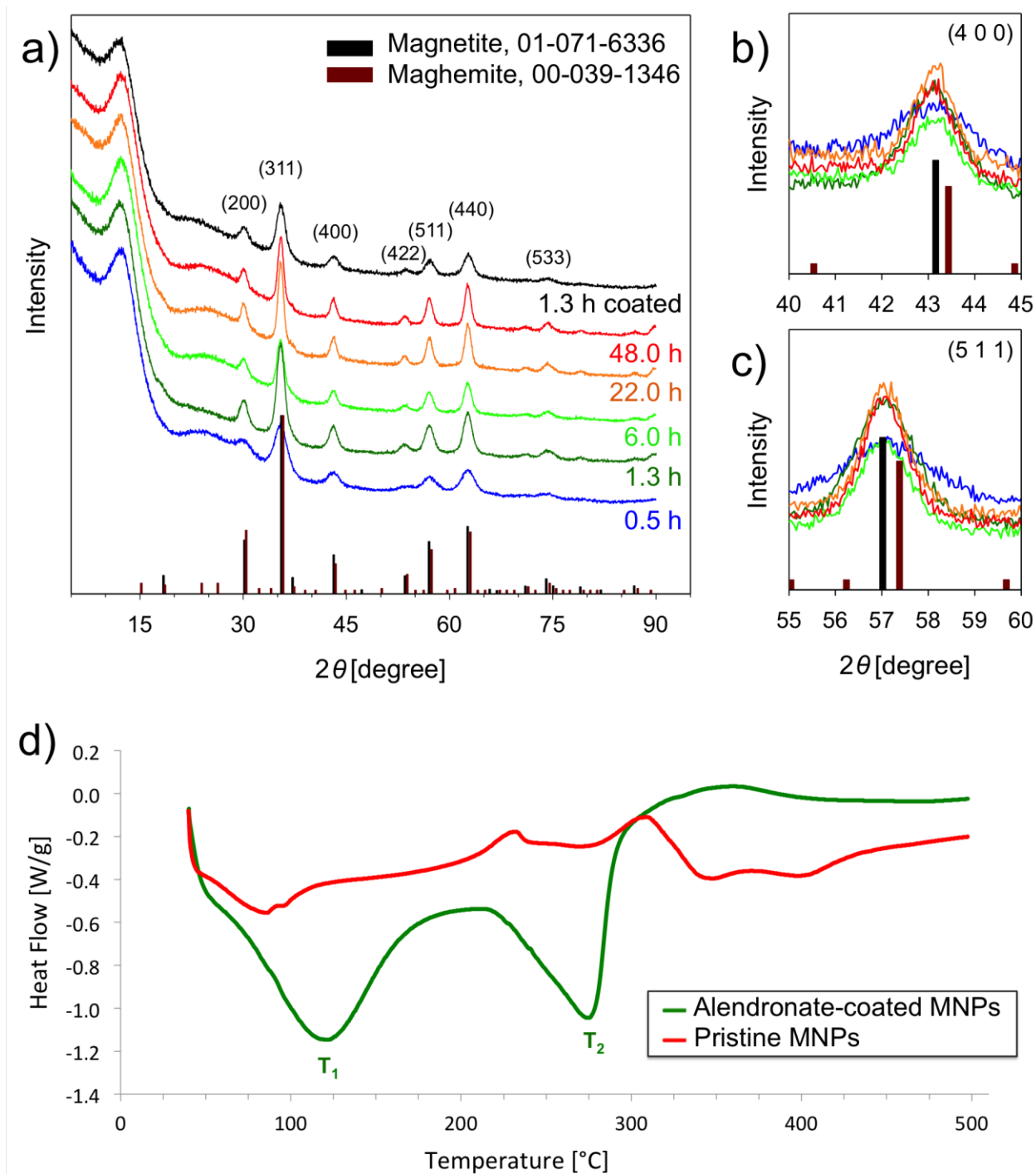
Figure 5. Results from the XRD and DSC studies. (a) Comparison of XRD pattern for samples with increasing heat duration (blue to red) to standard patterns provided by NIST for magnetite (black bars) and maghemite (brown bars). Also shown are the patterns for an

alendronate-coated MNP sample after 1.3 h synthesis. Numbers in parentheses represent identified peaks. (b,c) Close-up comparison of two characteristic peaks indicates that the sample contains mainly magnetite. (d) Results from DSC Analysis for MNPs synthesized over 1.3 h. Shown are the heat flow curves for pristine MNPs (red curve) and MNPs coated with alendronate (green curve).

DSC Analysis

The endothermic heat flow shows two pronounced peaks (labeled T1 and T2 in **Fig. 5d**) in alendronate-coated MNPs, which indicate some magnetite to maghemite transition [34]. It has to be noted, however, that no oxygen was used for oxidation and only nitrogen flow was supplied during the DSC analysis. It can be speculated that the exothermic transition T1 can be associated to magnetite to maghemite transition at the particle surface. Alternatively, the exothermic transition can be a result from water evaporation from the particle's surface or a degradation of the bisphosphonate coating. The transition is not present in the pristine MNPs (red line in **Fig. 5d**), indicating that the surface modification with alendronate may cause the change in transition. However, a transitional component of magnetite/maghemite in alendronate coated MNPs was not found in our XRD study. This could be due to additional effects that are measurable by DSC but not by XRD analysis. Further studies will be required to elucidate the findings from the DSC analysis. However, such studies are beyond the scope of our current investigation.

CONCLUSIONS

Rapid and facile synthesis of magnetic nanoparticles is a major challenge to the development of magnetic drug carriers. We showed here a simple method based on a low cost iron precursor material (iron acetylacetonate), a green solvent (TEG), and microwave based heating to create magnetite MNPs with small sizes and high saturation magnetization. The MNPs showed minimal batch-to-batch variability, minimal variation in particle size at short reaction durations, and the use of polyols as solvent was found to be beneficial for minimizing toxicity of the MNPs. Our study showed no toxicological effect of pristine MNPs at concentrations of up to 100 μg Fe / mL, which is comparable to similar studies using MTT assays, albeit for different cell lines used in those studies [30].

The use of water miscible polyols, such as TEG, is beneficial to advance the particle synthesis and coating towards a truly one-pot synthetic method. Conventional methods rely on lengthy washing and purification steps after completion of the particle synthesis. Additional intermediate wet chemical steps are often required to overcome challenges in the immiscibility between solvents, particles, and coating materials. The use of TEG in combination with solvothermal synthesis resulted in small MNPs with narrow size distributions as shown by DLS and TEM measurements. We showed here the successful coating of MNPs directly in the solvent used to synthesize the MNPs. This direct coating required no sample transfer and the successful coating was verified by changes in the FT-IR spectra of the MNPs and by changes in the particle's surface charges which is consistent with studies using similar bisphosphonate coating strategies [31,35]. The resulting alendronate-MNPs are functionalized, easily removed from the solvent by either dilution and magnetic separation or precipitation and centrifugation.

Together with the scalability of the synthesis the method presented here is ideal for rapid high throughput synthesis. We showed that by increasing the reaction volume and the precursor

concentration, the particle throughput can be scaled from milligrams to grams with high $M_{sat}$. The scalability of the synthesis showed an increase in particle size dispersity, which can be attributed to the process control of the microwave synthesizer. An improvement to the temperature control in large glass vials used for synthesis is expected to address the dispersity increase with increased reaction volume, resulting in fully scalable MNP synthesis without changes to the MNP size distribution.

The particles showed increasing saturation magnetization with increasing heating duration and were mainly composed of magnetite. The small particle size and the magnetite composition is an essential requirement for the use of such MNPs as magnetic drug carriers. The particles' superparamagnetic behavior as shown in our magnetic characterization will minimize or eliminate particle agglomeration after the particles are removed from the magnetic field. This is of great importance for therapies *in vivo* to minimize the risk of arterial clogging by the magnetic drug carriers. The potential of a scale-up in reaction volume and particle weight is a great benefit to the microwave synthesis method. The reaction times investigated in this study spanned more than two orders of magnitude and the resulting increase in saturation magnetization ($M_{sat}$) of the final MNPs was not linear. The greatest change $M_{sat}$ was observed for an increase of reaction time from 30 min to 1.3 h (32%) and the subsequent change in $M_{sat}$ falls to 3% for an increase in the reaction time from 22.3 h to 48.3 h. Depending on the final application of the MNPs synthesized by this method, the benefit of scalability of this method in green solvents can be paired with relative short reaction durations (*i.e.*, few min to 1 h) and clearly show the advantages over conventional methods.

**Supporting Information Available:**

Additional figure from size distribution analysis based on VSM measurements from scale up experiments (S1).

**Abbreviations Used**

Coefficient of variation, CV; Differential Scanning Calorimetry, DSC; dynamic light scattering, DLS; Fourier-Transform Infrared, FT-IR; Magnetic Nanoparticle, MNP; saturation magnetization, $M_{sat}$; Superconducting Quantum Interference Device, SQUID; Transmission Electron Microscopy, TEM; Triethylene glycol, TEG; Vibrational sample magnetometry, VSM; X-Ray Diffraction, XRD

**Notes:**

The authors declare no competing financial interest(s).

**Acknowledgements**

**References**

[1]     C. Alexiou, R. Jurgons, R.J. Schmid, C. Bergemann, J. Henke, W. Erhardt, E. Huenges, F. Parak, Magnetic drug targeting--biodistribution of the magnetic carrier and the chemotherapeutic agent mitoxantrone after locoregional cancer treatment., J. Drug Target. 11 (2003) 139–149. doi:10.3109/1061186031000150791.

[2]     C. Alexiou, R.J. Schmid, R. Jurgons, M. Kremer, G. Wanner, C. Bergemann, E. Huenges, T. Nawroth, W. Arnold, F.G. Parak, Targeting cancer cells: Magnetic nanoparticles as drug carriers, Eur. Biophys. J. 35 (2006) 446–450. doi:10.1007/s00249-006-0042-1.

[3]     T. Schneider, U.O. Hafeli, Magnetic Drug Delivery, in: A. Ionescu, N. Darton, J. Llandro (Eds.), Magn. Nanoparticles Biosensing Med., Cambridge University Press, 2017: pp. 300, in press (ISBN: 978–1–107–03109–8).

[4]     L. Sun, L. Zhan, Y. Shi, L. Chu, G. Ge, Z. He, Microemulsion synthesis and electromagnetic wave absorption properties of monodispersed Fe3O4/polyaniline core-shell nanocomposites, Synth. Met. 187 (2014) 102–107. doi:10.1016/j.synthmet.2013.11.007.

[5]     X. Wang, J. Zhuang, Q. Peng, Y. Li, A general strategy for nanocrystal synthesis., Nature. 437 (2005) 121–124. doi:10.1038/nature03968.

[6]     A.H. Lu, E.L. Salabas, F. Schüth, Magnetic nanoparticles: Synthesis, protection,

        functionalization, and application, Angew. Chemie - Int. Ed. 46 (2007) 1222–1244.

        doi:10.1002/anie.200602866.

[7]     S. Sun, Monodisperse FePt Nanoparticles and Ferromagnetic FePt Nanocrystal

        Superlattices, Science (80-. ). 287 (2000) 1989–1992. doi:10.1126/science.287.5460.1989.

[8]     S. Sun, H. Zeng, D.B. Robinson, S. Raoux, P.M. Rice, S.X. Wang, G. Li, Monodisperse

        MFe2O4 (M = Fe, Co, Mn) nanoparticles., J. Am. Chem. Soc. 126 (2004) 273–279.

        doi:10.1021/ja0380852.

[9]     F.X. Redl, C.T. Black, G.C. Papaefthymiou, R.L. Sandstrom, M. Yin, H. Zeng, C.B.

        Murray, S.P. O'Brien, Magnetic, electronic, and structural characterization of

        nonstoichiometric iron oxides at the nanoscale, J. Am. Chem. Soc. 126 (2004) 14583–

        14599. doi:10.1021/ja046808r.

[10]    D. Arndt, V. Zielasek, W. Dreher, M. Bäumer, Ethylene diamine-assisted synthesis of iron

        oxide nanoparticles in high-boiling polyolys, J. Colloid Interface Sci. 417 (2014) 188–

        198. doi:10.1016/j.jcis.2013.11.023.

[11]    M. Niederberger, N. Pinna, Metal Oxide Nanoparticles in Organic Solvents - Synthesis,

        Formation, Assembly and Application, Springer-Verlag, London, 2009.

[12]    C. Blanco-Andujar, D. Ortega, P. Southern, Q. a Pankhurst, N.T.K. Thanh, High

        performance multi-core iron oxide nanoparticles for magnetic hyperthermia: microwave

        synthesis, and the role of core-to-core interactions., Nanoscale. 7 (2015) 1768–75.

        doi:10.1039/c4nr06239f.

[13]    D. Adam, Microwave chemistry: Out of the kitchen., Nature. 421 (2003) 571–572.

doi:10.1038/421571a.

[14]    F. Benyettou, E. Guenin, Y. Lalatonne, L. Motte, Microwave assisted nanoparticle surface

functionalization., Nanotechnology. 22 (2011) 055102. doi:10.1088/0957-

4484/22/5/055102.

[15]    F. Benyettou, I. Milosevic, J.C. Olsen, L. Motte, A. Trabolsi, Ultra-Small

Superparamagnetic Iron Oxide Nanoparticles Made to Order, Bioanal. Biomed. S5 (2012)

6. doi:10.4172/1948-593X.S5-006.

[16]    O. Orliac, A. Rouilly, F. Silvestre, L. Rigal, Effects of various plasticizers on the

mechanical properties, water resistance and aging of thermo-moulded films made from

sunflower proteins, Ind. Crops Prod. 18 (2003) 91–100. doi:10.1016/S0926-

6690(03)00015-3.

[17]    V. Piemonte, M. Maschietti, F. Gironi, A Triethylene Glycol–Water System: A Study of

the TEG Regeneration Processes in Natural Gas Dehydration Plants, Energy Sources, Part

A Recover. Util. Environ. Eff. 34 (2012) 456–464. doi:10.1080/15567031003627930.

[18]    J.G. Schier, D.B. Barr, Z. Li, A.F. Wolkin, S.E. Baker, L.S. Lewis, M. a. McGeehin,

Diethylene Glycol in Health Products Sold Over-the-Counter and Imported from Asian

Countries, J. Med. Toxicol. 7 (2011) 33–38. doi:10.1007/s13181-010-0111-9.

[19]    L. Imbert, E. Saussereau, C. Lacroix, Analysis of eight glycols in serum using LC-ESI-

MS-MS, J. Anal. Toxicol. 38 (2014) 676–680. doi:10.1093/jat/bku100.

[20]    I.-M. Grabs, C. Bradtmöller, D. Menzel, G. Garnweitner, Formation Mechanisms of Iron

Oxide Nanoparticles in Different Nonaqueous Media, Cryst. Growth Des. 12 (2012)

1469–1475. doi:10.1021/cg201563h.

[21]   M. Kraken, I.C. Masthoff, A. Borchers, F.J. Litterst, G. Garnweitner, Formation of
       magnetic nanoparticles studied during the initial synthesis stage, Hyperfine Interact. 224
       (2014) 57–63. doi:10.1007/s10751-013-0767-z.

[22]   I.-C. Masthoff, F. David, C. Wittmann, G. Garnweitner, Functionalization of magnetic
       nanoparticles with highbinding capacity for affinity separation of therapeutic proteins, J.
       Nanopart. Res. 16 (2014) 2164. doi:10.1007/s11051-013-2164-6.

[23]   L. Suber, G. Marchegiani, E.S. Olivetti, F. Celegato, M. Coïsson, P. Tiberto, P. Allia, G.
       Barrera, L. Pilloni, L. Barba, F. Padella, P. Cossari, A. Chiolerio, Pure magnetic hard fct
       FePt nanoparticles: Chemical synthesis, structural and magnetic properties correlations,
       Mater. Chem. Phys. 144 (2014) 186–193. doi:10.1016/j.matchemphys.2013.12.041.

[24]   E. Carenza, V. Barceló, A. Morancho, J. Montaner, A. Rosell, A. Roig, Rapid synthesis of
       water-dispersible superparamagnetic iron oxide nanoparticles by a microwave-assisted
       route for safe labeling of endothelial progenitor cells, Acta Biomater. 10 (2014) 3775–
       3785. doi:10.1016/j.actbio.2014.04.010.

[25]   E. Solano, C. Frontera, T. Puig, X. Obradors, S. Ricart, J. Ros, Neutron and X-ray
       diffraction study of ferrite nanocrystals obtained by microwave-assisted growth. A
       structural comparison with the thermal synthetic route, in: J. Appl. Cryst., 2014: pp. 414–
       420. doi:10.1107/S1600576713032895.

[26]   S.S. Pati, S. Kalyani, V. Mahendran, J. Philip, Microwave assisted synthesis of magnetite
       nanoparticles, J. Nanosci Nanotechnol. 14 (2014) 5790–5797.
       doi:10.1016/j.jmmm.2011.08.029.

[27]   S. Kalyani, J. Sangeetha, J. Philip, Microwave Assisted Synthesis of Ferrite

Nanoparticles: Effect of Reaction Temperature on Particle Size and Magnetic Properties, J. Nanosci. Nanotechnol. 15 (2015) 5768–5774. doi:10.1166/jnn.2015.10274.

[28]    M. Brinkley, A brief survey of methods for preparing protein conjugates with dyes, haptens, and cross-linking reagents., Bioconjug. Chem. 3 (1992) 2–13. doi:10.1021/bc00013a001.

[29]    T. Weser, K. Stierstadt, Magnetoviscosity of concentrated ferrofluids, Z. Phys. B - Condens. Matter. 59 (1985) 257–260. doi:10.1007/BF01307428.

[30]    O. Bomati-Miguel, N. Miguel-Sancho, I. Abasolo, A.P. Candiota, A.G. Roca, M. Acosta, S. Schwartz, C. Arus, C. Marquina, G. Martinez, J. Santamaria, Ex vivo assessment of polyol coated-iron oxide nanoparticles for MRI diagnosis applications: Toxicological and MRI contrast enhancement effects, J. Nanoparticle Res. 16 (2014). doi:10.1007/s11051-014-2292-7.

[31]    F. Benyettou, Y. Lalatonne, I. Chebbi, M. Di Benedetto, J.-M. Serfaty, M. Lecouvey, L. Motte, A multimodal magnetic resonance imaging nanoplatform for cancer theranostics., Phys. Chem. Chem. Phys. 13 (2011) 10020–10027. doi:10.1039/c0cp02034f.

[32]    A.G. Roca, M.P. Morales, K. O'Grady, C.J. Serna, Structural and magnetic properties of uniform magnetite nanoparticles prepared by high temperature decomposition of organic precursors, Nanotechnology. 17 (2006) 2783–2788. doi:10.1088/0957-4484/17/11/010.

[33]    W. Kim, C.-Y. Suh, S.-W. Cho, K.-M. Roh, H. Kwon, K. Song, I.-J. Shon, A new method for the identification and quantification of magnetite–maghemite mixture using conventional X-ray diffraction technique, Talanta. 94 (2012) 348–352. doi:10.1016/j.talanta.2012.03.001.

[34]  H. V Lauer  Jr., D.W. Ming, D.C. Golden, E. Stansbery, Thermal Characterization of

Fe3O4 Nanoparticles Formed from Poorly Crystalline Siderite, in: 36th Lunar Planet. Sci.

Conf., 2005: p. 2153. http://adsabs.harvard.edu/abs/2005LPI....36.2153L.

[35]  F. Benyettou, Y. Lalatonne, O. Sainte-Catherine, M. Monteil, L. Motte,

Superparamagnetic nanovector with anti-cancer properties: gamma Fe2O3@Zoledronate.,

Int. J. Pharm. 379 (2009) 324–327. doi:10.1016/j.ijpharm.2009.04.010.



Table of Content Figure.

Highlights:

- Rapid and facile synthesis of magnetic nanoparticles
- Microwave synthesis in green solvent
- Magnetite MNPs with small sizes and high saturation magnetization
- Tunable particle properties depending on heating duration
- Scalable MNP synthesis